MCB
Journals.ASM.org

SWI/SNF Chromatin-Remodeling Factor Smarcd3/Baf60c Controls Epithelial-Mesenchymal Transition by Inducing Wnt5a Signaling

Nicole Vincent Jordan,[a] Aleix Prat,[b]* Amy N. Abell,[a]* Jon S. Zawistowski,[a] Noah Sciaky,[a] Olga A. Karginova,[b] Bingying Zhou,[a] Brian T. Golitz,[c] Charles M. Perou,[b] Gary L. Johnson[a]

Department of Pharmacology and Lineberger Comprehensive Cancer Center,[a] Department of Genetics and Lineberger Comprehensive Cancer Center,[b] and Department of Pharmacology and RNAi Screening Facility,[c] University of North Carolina School of Medicine, Chapel Hill, North Carolina, USA

We previously identified a gene signature predicted to regulate the epithelial-mesenchymal transition (EMT) in both epithelial tissue stem cells and breast cancer cells. A phenotypic RNA interference (RNAi) screen identified the genes within this 140-gene signature that promoted the conversion of mesenchymal epithelial cell adhesion molecule-negative (EpCAM$^-$) breast cancer cells to an epithelial EpCAM$^{+/high}$ phenotype. The screen identified 10 of the 140 genes whose individual knockdown was sufficient to promote EpCAM and E-cadherin expression. Among these 10 genes, RNAi silencing of the SWI/SNF chromatin-remodeling factor Smarcd3/Baf60c in EpCAM$^-$ breast cancer cells gave the most robust transition from the mesenchymal to epithelial phenotype. Conversely, expression of Smarcd3/Baf60c in immortalized human mammary epithelial cells induced an EMT. The mesenchymal-like phenotype promoted by Smarcd3/Baf60c expression resulted in gene expression changes in human mammary epithelial cells similar to that of claudin-low triple-negative breast cancer cells. These mammary epithelial cells expressing Smarcd3/Baf60c had upregulated Wnt5a expression. Inhibition of Wnt5a by either RNAi knockdown or blocking antibody reversed Smarcd3/Baf60c-induced EMT. Thus, Smarcd3/Baf60c epigenetically regulates EMT by activating WNT signaling pathways.

The epithelial-mesenchymal transition (EMT) is a reversible developmental process, whereby epithelial cells lose cell-cell adhesion and apical-basolateral polarity, while acquiring a mesenchymal front-back polarity and increased cellular invasiveness (1). During metastatic tumor progression, this developmental program becomes reactivated to confer tumor cells with enhanced migratory and invasive properties (2, 3). The opposing process of mesenchymal-epithelial transition (MET) reestablishes the epithelial state, as demonstrated by formation of epithelial tissues and organs in development and by metastatic colonization of epithelial tumors to distant organs (4). Understanding the molecular mechanisms controlling EMT, and the reverse process of MET, is important for development of new therapeutic strategies for the prevention and treatment of metastatic cancer and many other diseases such as organ fibrosis and impaired wound healing (5).

Cells undergoing EMT maintain the same genomic background in both mesenchymal and epithelial states, but during the progression of EMT, the gene expression profile significantly changes. The onset of EMT involves the repression of epithelium-specific genes and activation of mesenchyme-specific genes (6). Changes in promoter-specific DNA methylation altered expression of microRNAs (miRNAs) and enhanced expression of the transcription factors Snail, Slug, and Twist contribute to the induction of EMT (7, 8). We recently defined a signaling network involving mitogen-activated protein kinase kinase kinase 4 (MAP3K4) and Jun N-terminal protein kinase (JNK) whose inhibition reprograms epithelial tissue stem cells to undergo an EMT (9). MAP3K4/JNK-mediated phosphorylation of the histone acetyltransferase CBP stimulated acetylation of specific lysine marks in histones H2A/H2B that served to maintain an epithelial phenotype. Loss of MAP3K4/JNK activation of CBP promoted EMT in these tissue stem cells. This study was the first to demonstrate how loss of histone H2A/H2B acetylation could induce cells to lose the epithelial phenotype and enter EMT (9). Gene expression analysis of epithelial stem cells entering EMT and the claudin-low subtype of triple-negative breast cancer discovered a statistically significant intersecting EMT gene signature (9). Claudin-low triple-negative breast cancers characteristically have EMT features, are resistant to therapy, and demonstrate a propensity to metastasize to the lung and brain parenchyma (10–13).

On the basis of the gene signature derived from the overlapping epithelial stem cell and claudin-low breast cancer expression profiles, we hypothesized that the 140 genes upregulated in the EMT signature functioned to promote the mesenchymal phenotype. Using SUM149 and SUM229 breast cancer cells that exist in culture as dual populations of epithelial cell adhesion molecule-negative (EpCAM$^-$) (mesenchymal-like) and EpCAM$^{+/high}$ (epithelial-like) cells, we designed a phenotypic RNA interference (RNAi) screen to identify individual genes whose targeted knockdown in EpCAM$^-$ cells promoted the EpCAM$^{+/high}$ epithelial phenotype (13–15). Using this RNAi strategy, the SWI/SNF chromatin-remodeling factor Smarcd3/Baf60c was identified as a novel regulator of EMT. While small interfering RNA (siRNA)-mediated knockdown of Smarcd3/Baf60c induced a MET in EpCAM$^-$

Received 25 October 2012 **Returned for modification** 6 December 2012
Accepted 21 May 2013
Published ahead of print 28 May 2013

Address correspondence to Gary L. Johnson, gary_johnson@med.unc.edu.
* Present address: Aleix Prat, Translational Genomics Unit, Vall d'Hebron Institute of Oncology, Barcelona, Spain; Amy N. Abell, Department of Biological Sciences, University of Memphis, Memphis, Tennessee, USA.

Supplemental material for this article may be found at http://dx.doi.org/10.1128/MCB.01443-12.

doi:10.1128/MCB.01443-12

SUM149 and SUM229 cells, expression of Smarcd3/Baf60c in human mammary epithelial cells (HMECs) promoted EMT. Smarcd3/Baf60c activated the EMT program in HMECs by epigenetic induction of Wnt5a signaling. These results define Smarcd3/Baf60c as important for maintenance of the EMT properties and mesenchymal phenotype of claudin-low EpCAM$^-$ SUM149 and SUM229 breast cancer cells.

MATERIALS AND METHODS

Cell lines, culture conditions, constructs, and transfections. The primary HMEC line, immortalized using the retrovirus pBabe-hygro-hTERT (hygro stands for hygromycin, and hTERT stands for human telomerase reverse transcriptase), was cultured as previously described (16). SUM149 and SUM229 breast cancer cells were cultured in HuMEC medium (Life Technologies; catalog no. 12752-010) containing 5% fetal bovine serum (FBS), 1% penicillin and streptomycin (PS) plus bovine pituitary extract and HuMEC supplement or Ham's F-12 medium containing 5% FBS, 1% PS plus 5 μg/ml insulin and 1 μg/ml hydrocortisone, respectively. 293T cells were cultured in Dulbecco's modified Eagle's high-glucose medium with 10% FBS and 1% PS. Transfection of 293T cells was performed in 15-cm dishes for 24 h with Lipofectamine Plus (Invitrogen) according to the manufacturer's specifications. The Smarcd3/Snail/Slug Gateway entry plasmid was subcloned into a lentiviral FLAG-Gateway destination vector. The lentiviral FLAG-Gateway destination vector was a kind gift from Ben Major.

Lentivirus production and infections of HMECs. To produce replication-incompetent lentivirus, 293T cells were cotransfected with either pGIPZ empty vector, FLAG-Smarcd3/Snail/Slug lentiviral Gateway constructs in combination with pMD2.G and psPAX2 (Addgene) using Lipofectamine Plus reagent (Invitrogen). Twenty-four hours later, the cell medium was changed. Viral supernatants were harvested at 48 h post-transfection by ultracentrifugation, and viral pellets were resuspended in 300 μl base medium. HMECs were infected overnight with 100 μl lentivirus in 6 μg/ml Polybrene. Puromycin (3 μg/ml) was used to select transduced cells. Selection was complete 7 days after infection. Expression of Smarcd3/Snail/Slug was measured by quantitative reverse transcription-PCR (qRT-PCR).

Fluorescence-activated cell sorting (FACS). Cells were trypsinized and filtered into single-cell suspensions, resuspended in Hanks' balanced salt solution containing 2% FBS (HF medium), and incubated with antibodies for 30 min at 4°C. Cells were stained with the following antibodies, antibodies directed against EpCAM-FITC (EpCAM conjugated to fluorescein isothiocyanate [FITC]) (catalog no. 10109; Stem Cell Technologies), EpCAM-APC (EpCAM conjugated to allophycocyanin [APC]) (catalog no. 347200; BD), Cd49f-PE-Cy5 (Cd49f conjugated to phycoerythrin [PE] and Cy5) (catalog no. 551129; BD), Cd44-APC (catalog no. 559942; BD), or Cd24-FITC (catalog no. 555427; BD). Unbound antibodies were washed from cells using HF medium. For analytical flow, cells were fixed with 3% paraformaldehyde and analyzed using a Beckman-Coulter CyAn instrument. For sterile live-cell flow cytometry, cells were sorted using a Sony iCyt/reflection instrument.

RNAi screening conditions, immunofluorescence, and high-content imaging. For the RNAi screen, EpCAM$^-$ SUM149 or SUM229 cells were reverse transfected in fibronectin-coated 96-well plates (Greiner) with 25 nM siRNA smart pools (Dharmacon) containing the combination of 4 different siRNA oligonucleotides for each target or control gene (siRNA targeting ubiquitin B [siUBB] for siRNA knockdown efficiency; siRNA targeting glyceraldehyde-3-phosphate dehydrogenase [siGAPDH] for a negative control; siRNA targeting Snail and Slug [siSnail/Slug] for a positive control). Target genes were plated in duplicate on three replicate plates, and control genes were plated 2 times for UBB, 6 times for GAPDH, and 8 times for Snail/Slug on three replicate plates. After 6 days in culture, cells were fixed with 3% paraformaldehyde, permeabilized with 0.1% Triton X, and stained with nuclear 4′,6′-diamidino-2-phenylindole (DAPI) stain, EpCAM (catalog no. 01420; Stem Cell Technologies) and E-cadherin (catalog no. 3195S; Cell Signaling) antibodies. EpCAM (conjugated to secondary Alexa Fluor 555) and E-cadherin (conjugated to secondary Alexa Fluor 488) fluorescence was measured using the high-content BD Pathway 855 microscope system. Changes in EpCAM and E-cadherin expression were quantitatively measured on a single-cell basis as a function of the percent change in cellular fluorescence using the CellProfiler image analysis software. Results were the compilation of two independent screens performed in triplicate.

Confocal imaging. ZO-1 (catalog no. 33 -9100; Invitrogen) immunofluorescence experiments were conducted with an Olympus FluoView 1000 laser scanning confocal microscope with 40× UPLFLN 1.3-numerical-aperture (NA) oil objective with lasers at 405 and 488 nm. Single *z*-plane images of Alexa Fluor 488 and DAPI channels (1× or 2.4× zoom) were acquired sequentially with identical laser transmissivity and photomultiplier tube (PMT) voltage settings, and 4-frame Kalman averaging.

Western blotting of whole-cell and nuclear lysates. Whole-cell and nuclear lysates were isolated as previously described (17). Western blots were performed with the following antibodies: antibodies to EpCAM (catalog no. 71916; Abcam), E-cadherin (catalog no. 610181; BD), fibronectin (catalog no. CP70; Calbiochem), N-cadherin (catalog no. 76057; Abcam), vimentin (catalog no. 5741S; Cell Signaling), γ-tubulin (catalog no. T6557; Sigma), FLAG (catalog no. M5 F4042/F7425; Sigma), Snail (catalog no. 3895S; Cell Signaling), Slug (catalog no. 9585S; Cell Signaling), Brg1 (catalog no. sc-17796X; Santa Cruz), Brm (catalog no. 15597; Abcam), phosphorylated protein kinase Cβ (phospho-PKCβ) (catalog no. 9371S; Cell Signaling), phospho-JNK (catalog no. 9251S; Cell Signaling), β-catenin (catalog no. C7207; Sigma), and Smarcd3/Baf60c. Smarcd3/Baf60c antibody was a kind gift from Lorenzo Puri.

ChIP assays. Chromatin immunoprecipitation (ChIP) assays were performed as previously described (9). ChIP assays were quantified by real-time PCR using ABsolute blue SYBR green PCR mix (Thermo Scientific) and the Applied Biosystems Fast 7500 real-time PCR system. Fold enrichment was determined by the $2^{-\Delta CT}$ method. PCR primers were designed to amplify approximately 75- to 100-bp fragments from genomic DNA using Primer Express 3.0 (Applied Biosystems). ChIP–qRT-PCR primers include the following: Cdh1 sense (5′-ACCCCCTCTC AGTGGCGT-3′) and antisense (5′-GGAGCGGGCTGGAGTCTG); Cd44 sense (5′-AGTGGATGGACAGGAGGATG-3′) and antisense (5′-T TATGTCCTTCTGGGCTCT); Cldn4 sense (5′-TCAGCCTTCCAGGTC CTCAA-3′) and antisense (5′-CCCCATGGAGGCCATTG-3′); Wnt5a sense (5′-CCTATTTTGCTCCCCGTT-3′) and antisense (5′-AAGAGTC AGCCCCAAATT-3′).

Invasion assays. Cells were plated on growth factor-reduced Matrigel (BD Biosciences)-coated 8-μm-pore Transwell chambers. After 24 h, invasion assays were terminated. Noninvading cells were removed from the top of the Transwells by washing and swabbing. Invasive cells were quantified by fixing chambers in 3% paraformaldehyde for 10 min and staining with nuclear DAPI stain. For each Transwell, five 10× fields were imaged and counted.

Real-time qRT-PCR. qRT-PCR was performed as previously described (9).

Agilent gene expression microarrays. Transfected and control HMEC lines were profiled as described previously using 44,000 (44K) human oligonucleotide microarrays (Agilent Technologies, Santa Clara, CA, USA) (13, 18). The probes or genes for all analyses were filtered by requiring the lowest normalized intensity values in both sample and control to be >10. The normalized $\log_2$ ratios (Cy5 sample/Cy3 control) of probes mapping to the same gene (Entrez identification [ID] as defined by the manufacturer) were averaged to generate independent expression estimates. At least three biological replicates were used for each transfected gene (i.e., each Cy5 sample). For Cy3 controls, we used the empty vector cell line, which was the same for all samples. All microarray data are available in the University of North Carolina (UNC) Microarray Database (https://genome.unc.edu/).

Gene signatures. The previously published claudin-low predictor and the differentiation score were evaluated as previously described (13). For each infected HMEC line (i.e., Smarcd3, Slug and Snail), we derived a gene signature by performing a one-class significance analysis of microarrays (SAM) with a false discovery rate of 0%. The resulting gene lists can be found in Table S4 in the supplemental material. An enrichment score for each individual signature (up- and downregulated genes combined) was evaluated in the previously published UNC337 data set (GSE18229) of breast cancer samples representing all the intrinsic molecular subtypes. To do so, we calculated the inner product of each signature (gene ratio) and the gene expression value of each breast tumor sample. Subtype calls in the UNC337 data set were used as provided in Gene Expression Omnibus (GEO) (13).

Statistical analysis. Gene overlap between two signatures was estimated using exact hypergeometric probabilities implemented in R package (http://cran.r-project.org). All microarray cluster analyses were displayed using Java Treeview version 1.1.4r2. Average-linkage hierarchical clustering was performed using Cluster v3.0 (19).

Microarray data accession number. All microarray data have been deposited in the GEO database under accession number GSE40145.

RESULTS

SUM149 and SUM229 breast cancer cells maintain epithelial and mesenchymal populations. SUM149 and SUM229 cells maintain two distinct populations of EpCAM$^-$ and EpCAM$^{+/high}$ cells with similar growth rates (Fig. 1A and B) that exhibit the profiles of claudin-low and basal-like breast cancer cells, respectively, by gene expression analysis (13). Gupta and colleagues modeled the behavior of the dual population in SUM149 cells as being in a phenotypic equilibrium with each other (14). Further characterization of the two populations revealed the mesenchymal versus epithelial characteristics of EpCAM$^-$ and EpCAM$^{+/high}$ cells, respectively. EpCAM$^-$ cells demonstrated a spindle-like mesenchymal morphology contrasting with the rounded epithelial morphology of the EpCAM$^{+/high}$ cells (Fig. 1C). Both EpCAM$^{+/high}$ cell lines express modest levels of E-cadherin with SUM149 cells having more expression of E-cadherin than SUM229 cells. Immunofluorescence and Western blotting confirmed the absence or low expression of the epithelial markers EpCAM and E-cadherin in EpCAM$^-$ SUM149 and SUM229 cells (Fig. 1C to E). Compared to EpCAM$^{+/high}$ cells, EpCAM$^-$ cells showed elevated protein expression of the mesenchymal markers fibronectin, N-cadherin, and vimentin (Fig. 1D and E) and had filamentous actin stress fibers consistent with a front-back end polarized mesenchymal phenotype (not shown). The mesenchymal phenotype was even more pronounced in the EpCAM$^-$ SUM229 cells than in the EpCAM$^{+/high}$ SUM229 cells. Changes in protein expression in EpCAM$^-$ cells versus EpCAM$^{+/high}$ cells were mirrored with decreased mRNA expression of the epithelial markers E-cadherin and EpCAM (Fig. 1F and G). There was also increased expression of the mesenchymal markers N-cadherin, vimentin, transforming growth factor β (TGF-β), and the EMT-inducing transcription factors Snail, Slug, and Twist in EpCAM$^-$ cells than in EpCAM$^{+/high}$ cells (Fig. 1F to I). Functionally, the EpCAM$^-$ SUM149 and SUM229 cells were 3- and 8-fold more invasive through growth factor-reduced Matrigel than the EpCAM$^{+/high}$ cells, respectively (Fig. 1J). These results demonstrated that the epithelial EpCAM$^{+/high}$ and mesenchymal EpCAM$^-$ populations of SUM149 and SUM229 cells are morphologically and functionally distinct.

RNAi screen identifies genes important for EMT. EpCAM$^-$ SUM149 and SUM229 cells were used in RNAi screens to identify genes important for maintenance of the mesenchymal phenotype (Fig. 2A). Fluorescence-activated cell sorting (FACS) purity checks before each screen showed less than 0.5% contamination of the EpCAM$^-$ population of cells with EpCAM$^{+/high}$ cells when the screens were initiated (Fig. 2B), indicating that increases in EpCAM and E-cadherin expression resulted from a cellular transition from the mesenchymal EpCAM$^-$ to epithelial EpCAM$^{+/high}$ state. Validation of our screen image analysis was achieved by titrating set percentages of EpCAM$^{+/high}$ SUM149 cells into an EpCAM$^-$ background. The percent cellular fluorescence of EpCAM and E-cadherin immunostaining assessed by high-content image analysis closely recapitulated the titrated percentages (not shown). This robust RNAi screening platform was used for identification of genes whose knockdown induced a mesenchymal to epithelial transition (MET) in EpCAM$^-$ SUM149 and SUM229 cells.

Pools of four independent siRNA oligonucleotides were used to individually target the 140 upregulated genes within the EMT gene signature shared by epithelial stem cells developmentally entering EMT and claudin-low breast cancer (see Table S1 in supplemental material) (9). With the exception of Slug, Twist, vimentin, and N-cadherin, these genes are uncharacterized with respect to EMT.

As proof of principle for the RNAi screening strategy, we silenced known EMT-inducing genes Snail and Slug and measured the increase in epithelial markers EpCAM and E-cadherin by immunofluorescence (Fig. 2C and D). These experiments demonstrated that siRNA-mediated knockdown of Snail or Slug in the mesenchymal EpCAM$^-$ SUM149 cells resulted in increased EpCAM and E-cadherin expression, loss of the mesenchymal phenotype, and gain of the epithelial phenotype within 6 days posttransfection (Fig. 2C to E). At 6 days posttransfection, control GAPDH siRNA-treated EpCAM$^-$ cells had a background of less than 3% EpCAM- or E-cadherin-positive cells (Fig. 2C and D). In contrast, dual knockdown of Snail and Slug resulted in 26 and 10% EpCAM or E-cadherin-positive SUM149 cells, respectively (Fig. 2D). A highly reproducible 3- to 5-fold change in EpCAM and E-cadherin percent fluorescence was observed with siRNA-mediated knockdown of Slug or Snail versus control GAPDH knockdown (Fig. 2D).

The RNAi screen targeted 140 upregulated genes within the EMT gene signature and identified 10 genes whose individual knockdown resulted in the morphological transition between EpCAM$^-$ and EpCAM$^{+/high}$ phenotypes in both SUM149 and SUM229 cells (Fig. 2F; see Table S2 in supplemental material). Compared to control GAPDH siRNA knockdown, siRNA-mediated knockdown of these 10 EMT regulatory genes demonstrated a statistically significant increase in the percent EpCAM and E-cadherin cellular fluorescence (Fig. 3A and B). The 10 identified EMT regulatory genes included the following: Slug, Cdh2, Smarcd3/Baf60c, ABR, Rnf130, EphA4, Met, Ptprb, Fhl1, and RRAGD (Fig. 3A to D; see Table S3 in supplemental material for gene functions). In addition to upregulation of EpCAM and E-cadherin protein expression, siRNA-mediated knockdown of these EMT regulatory genes induced morphological changes characteristic of an epithelial, cobblestone morphology.

Of the 10 EMT regulatory genes identified in the phenotypic RNAi screen, five genes, including Cdh2, Smarcd3/Baf60c, Fhl1, Rnf130, and RRAGD were upregulated in the mesenchymal EpCAM$^-$ cells relative to the epithelial EpCAM$^{+/high}$ SUM149 and SUM229 cells (Fig. 4A). Deconvolution of siRNA oligonucle-

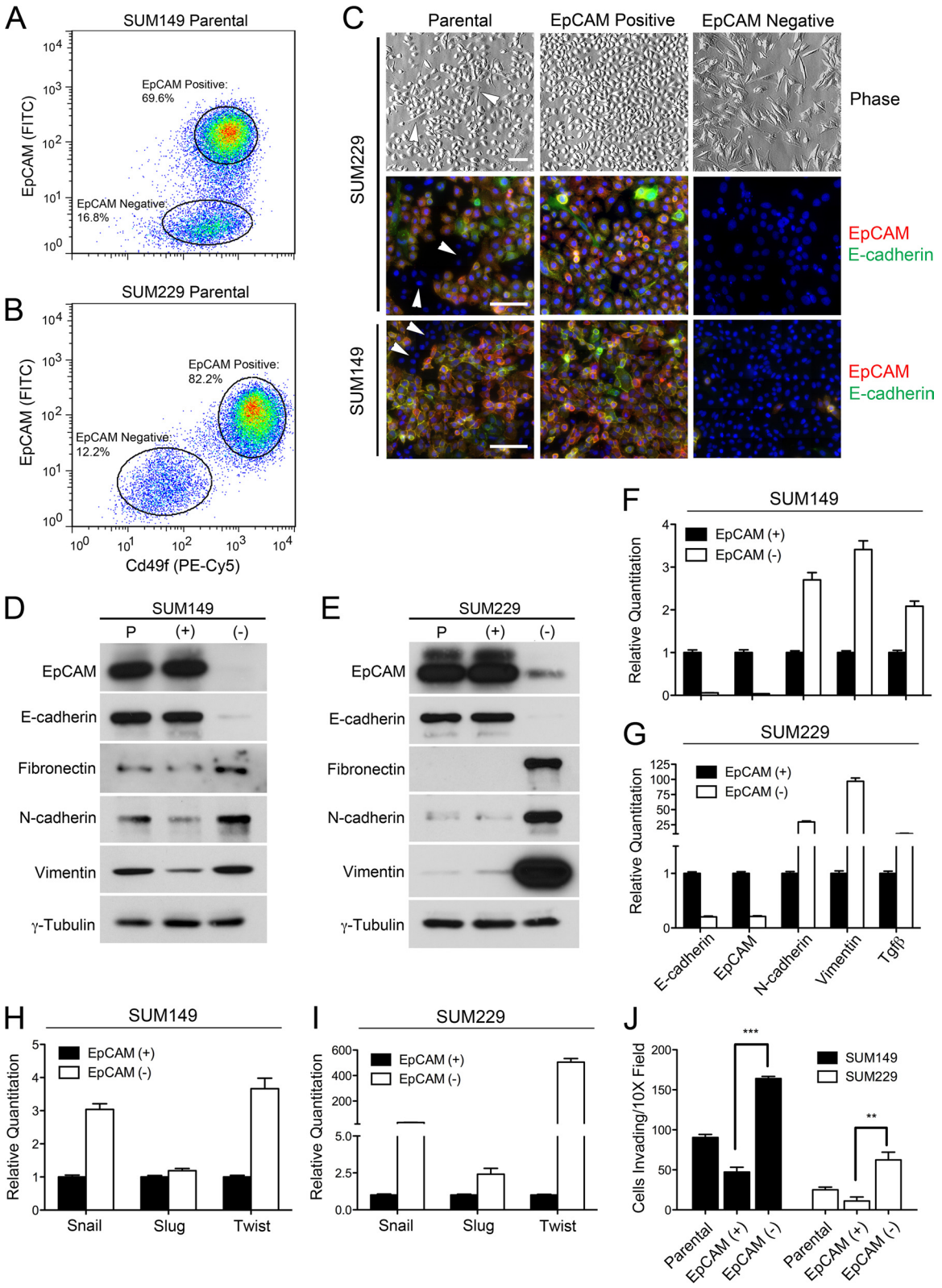

FIG 1 SUM149 and SUM229 breast cancer cells maintain epithelial and mesenchymal populations. (A and B) FACS analysis of SUM149 and SUM229 cells showing EpCAM$^-$ and EpCAM$^{+/high}$ populations. (C) Epithelial and mesenchymal properties of EpCAM$^{+/high}$ and EpCAM$^-$ populations shown by phase microscopy and immunostaining with nuclear DAPI (blue) stain and anti-E-cadherin (green) and anti-EpCAM (red) antibodies. Arrowheads indicate the EpCAM$^-$ cells in the parental SUM229 and SUM149 cell lines. Bars, 100 μm. (D and E) Reduced EpCAM and E-cadherin protein expression with elevated fibronectin, N-cadherin, and vimentin protein in EpCAM$^-$ cells. The presence and level of various proteins in the parental (P), EpCAM$^{+/high}$ (+), and EpCAM$^-$ (−) SUM149 (E) and SUM229 (F) breast cancer cells are shown. The data in panels A to E are representative of the data from at least two independent

otide pools for each of the 10 genes showed efficient knockdown of the EMT regulatory target genes by at least two of the four oligonucleotides, consistent with increases in EpCAM and E-cadherin expression being the result of on-target knockdown (Fig. 4B). Functionally, knockdown of ABR, Cdh2, Smarcd3/Baf60c, or Slug expression resulted in significant decreases in cellular invasiveness through growth factor-reduced Matrigel (Fig. 4C; see Table S3 in supplemental material). RNAi knockdown of several of the EMT regulatory genes induced a decrease in mRNA expression of the EMT-inducing transcription factors Snail and Slug (Fig. 4D and E; see Table S3). Thus, the RNAi screen effectively identified genes whose selective loss was sufficient to promote the epithelial phenotype of SUM149 and SUM229 breast cancer cells.

Smarcd3/Baf60c is an epigenetic regulator of EMT. Of the EMT regulatory genes identified in the screen, RNAi silencing of the SWI/SNF chromatin-remodeling factor Smarcd3/Baf60c in EpCAM$^-$ breast cancer cells gave the most robust transition from the mesenchymal to epithelial phenotype. Smarcd3/Baf60c has the potential to affect a broad network of genes through its epigenetic regulatory function as a member of the SWI/SNF chromatin-remodeling complex (20–23). The specificity of the Smarcd3/Baf60c knockdown was demonstrated by rescue of the EpCAM$^-$ phenotype by transfection of a siRNA resistant to knockdown (Fig. 5A and B), indicating that the increases in EpCAM and E-cadherin expression resulted from targeted Smarcd3/Baf60c knockdown and not an off-target response to the siRNA.

To determine its role in the regulation of EMT, FLAG-tagged Smarcd3/Baf60c was stably expressed in human mammary epithelial cells (HMECs) at levels comparable to mesenchymal EpCAM$^-$ SUM149 cells (Fig. 5C). HMECs expressing Smarcd3/Baf60c (D3-HMECs) demonstrated phenotypic changes indicative of EMT (Fig. 5D). D3-HMECs lost their epithelial cell morphology and became mesenchymal cell-like, with diminished expression of epithelial cell-cell adhesion markers EpCAM and E-cadherin and gain of expression of the mesenchymal marker vimentin (Fig. 5D). Western blotting confirmed the decreased expression of EpCAM and E-cadherin with gain of fibronectin and vimentin (Fig. 5E). Of the EMT-inducing transcription factors, Lef1 and Zeb2 mRNAs were increased compared to empty vector control HMECs (EV-HMECs) (Fig. 5F). Furthermore, the epithelial cell-cell adhesion genes E-cadherin, EpCAM, Krt7, Krt19, Cldn4, and Cldn7 were downregulated (Fig. 5F). Notably, mRNA expression of the tight junction genes Cldn4 and Cldn7 was reduced 90% compared to EV-HMECs. EV-HMECs and D3-HMECs when analyzed by FACS, profiled as separate cellular populations based on antigenic expression levels of epithelial differentiation markers EpCAM/Cd49f and breast cancer stem cell markers Cd44/Cd24. Compared to EV-HMECs, the D3-HMECs demonstrated a reduction in the epithelial integrin Cd49f and gain in the prometastatic glycoprotein Cd44 with no change in the prodifferentiation glycoprotein Cd24 (Fig. 5G). D3-HMECs also showed increased cytoplasmic staining of the tight junctions protein zona occludins (ZO-1) compared to EV-HMECs (Fig. 5H). The changes in ZO-1 staining were accompanied with a loss of epithelial cobblestone morphology and tight junctions (Fig. 5H). These results support the role of Smarcd3/Baf60c as an EMT-inducing chromatin-remodeling factor that promotes loss of the epithelial phenotype by a reduction in cell-cell adhesions with gain of the mesenchymal phenotype.

Smarcd3/Baf60c expression in HMECs induces a claudin-low gene signature. We performed gene arrays to measure expression changes in D3-HMECS relative to EV-HMECs. Additionally, we compared gene expression changes of D3-HMECS with Snail- and Slug-expressing HMECs (Snail-HMECs and Slug-HMECs, respectively) to define gene networks important for EMT. Hierarchical cluster analysis of gene array data from D3-, Slug-, and Snail-HMECs with respect to the 9-cell line claudin-low predictor described by Prat et al. (13) revealed that the gene expression profiles of D3-HMECs clustered similarly to the claudin-low signature of human breast cancer (Fig. 6A and B; see Table S4 in supplemental material). Conversely, the gene expression profiles of Slug- and Snail-HMECs demonstrated substantially less overlap with the claudin-low signature (Fig. 6A and B; see Table S4). Of the D3-, Slug-, and Snail-HMECs, D3-HMECs had the most significant gene intersection (P value < 0.0001) with the claudin-low signature sharing 7% upregulated and 13% downregulated genes (Fig. 6B; see Table S4). D3- and Slug-HMECs shared a significant gene intersection (P value < 0.0001) with 41% upregulated and 18% downregulated shared genes (Fig. 6C; see Table S4), suggesting that Smarcd3/Baf60c and Slug affect an overlapping EMT gene network. To further emphasize the significance of the D3-HMEC/claudin-low association, the gene expression profile of D3-HMECs was compared to the five intrinsic molecular subtypes of human breast tumors catalogued in the UNC337 data set. Tumors from the claudin-low subtype showed highest expression of the D3-HMEC signature in comparison with basal-like, HER2-enriched, luminal A and luminal B tumors (Fig. 6D). The differentiation predictor described by Prat et al. (13), which uses gene expression profiles to determine the cellular relatedness to the normal breast epithelial differentiation hierarchy from mammary stem cells (MaSCs) to mature luminal cells showed that D3-HMECs had the lowest differentiation score compared to Slug- and Snail-HMECs (Fig. 6E) (24). This suggests that D3-HMECs profile more similarly to MaSCs and more importantly to a less-differentiated mesenchymal, claudin-low phenotype than Slug- and Snail-HMECs. Collectively, these findings demonstrate that Smarcd3/Baf60c induces an EMT gene expression program in HMECs similar to that of the claudin-low breast cancer subtype.

Molecular characterization of the Smarcd3/Baf60c-induced EMT in HMECs showed a more profound phenotypic conversion than that of the Snail- or Slug-induced EMT in HMECs. Morphological changes included a loss of cell-cell adhesions in D3-HMECs, whereas Snail- and Slug-HMECs maintained a partial degree of epithelial cell-cell adhesions through either E-cadherin

experiments. (F and G) Reduced EpCAM and E-cadherin mRNA expression and elevated N-cadherin, vimentin, and TGFβ expression in EpCAM$^-$ cells than in EpCAM$^{+/high}$ cells. (H and I) Elevated mRNA expression of EMT-inducing transcription factors Snail, Slug, and Twist in EpCAM$^-$ cells compared to EpCAM$^{+/high}$ cells measured by qRT-PCR. The values in panels F to I are means plus standard errors of the means (SEMs) (error bars) of three independent experiments performed in triplicate. (J) Increased invasiveness of mesenchymal EpCAM$^-$ compared to epithelial EpCAM$^{+/high}$ cells through growth factor-reduced Matrigel-coated Transwell chambers. Statistical significance was evaluated by an unpaired Student's t test and indicated as follows: ***, P value < 0.001; **, P value < 0.01. Values are means plus SEMs of two independent experiments performed in triplicate.

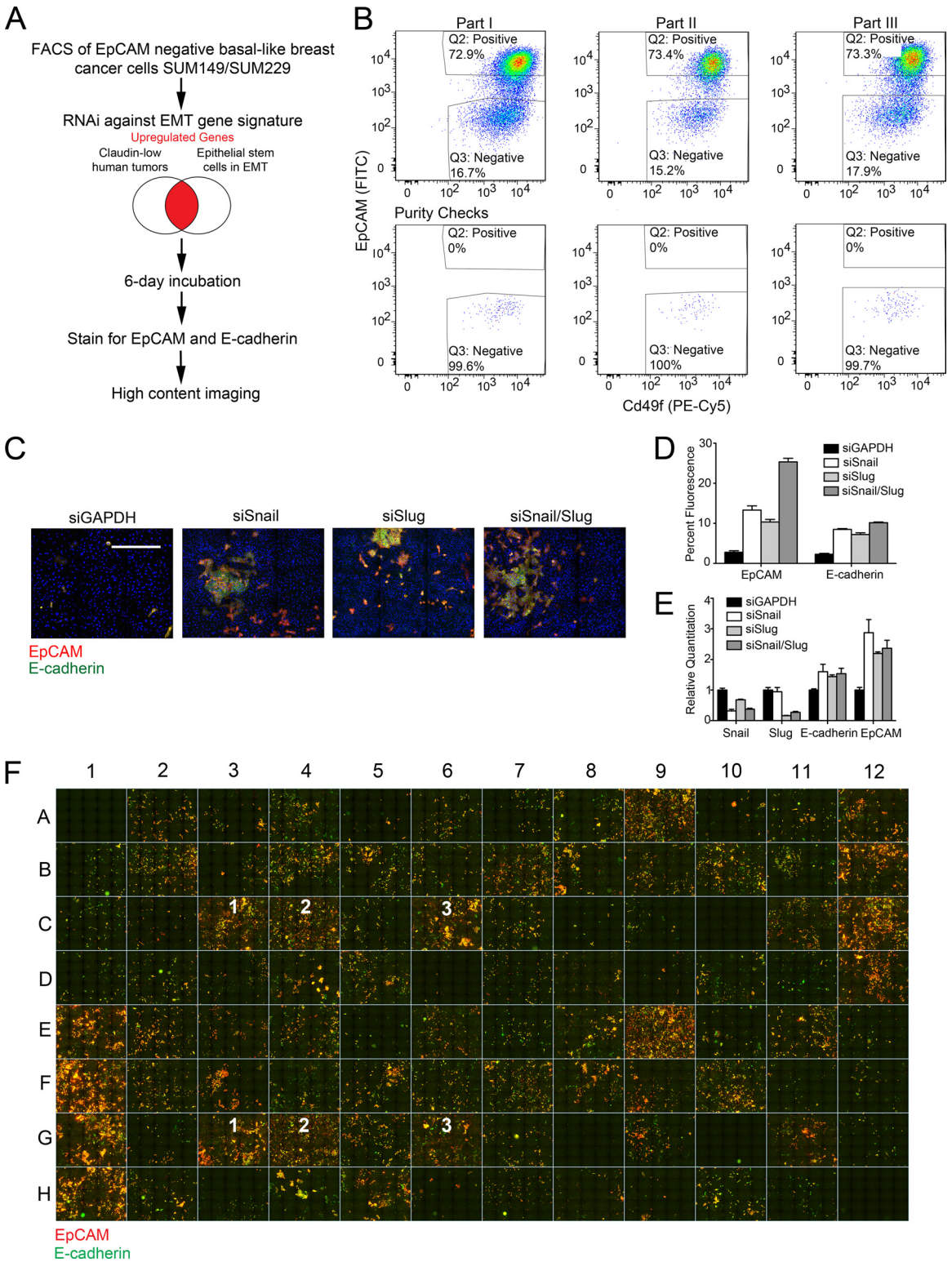

FIG 2 RNAi screening strategy for EMT regulatory genes. (A) Schematic depicting the RNAi screening strategy. (B) Separation of EpCAM$^{+/high}$ and EpCAM^{-} SUM149 cells by FACS shows less than 0.5% EpCAM$^{+/high}$ contamination in the EpCAM^{-} cells. Data depict FACS analysis of three individual cell sorts used for the primary RNAi screen. Q2, quadrant 2. (C) Acquisition of the epithelial phenotype by mesenchymal EpCAM^{-} cells following siRNA-mediated knockdown of Snail, Slug, or both Snail/Slug genes as shown by immunostaining with nuclear DAPI (blue) stain, anti-E-cadherin (green), and anti-EpCAM (red) antibodies. Bar, 500 μm. (D) Elevated EpCAM and E-cadherin percent cellular fluorescence quantitated on a single-cell basis following siRNA-mediated knockdown of the genes indicated. Values are means plus SEMs (error bars) of 8 independent wells. (E) Elevated mRNA expression of epithelial markers EpCAM and E-cadherin following siRNA-mediated knockdown of Snail and Slug measured by qRT-PCR. Values are means plus SEMs of three independent experiments performed in triplicate. (F) Representative plate image from the RNAi screen shows expression of epithelial markers E-cadherin (green) and EpCAM (red) by immunofluorescence in EpCAM^{-} SUM149 cells following siRNA-mediated knockdown of target genes in duplicate wells shown in columns 2 to 11 in rows A to H; siGAPDH in columns 1 and 12, rows B to D and E to H, respectively; siSnail/Slug in columns 1 and 12, rows E to H and A to D, respectively; and siUBB in wells A1 and H12. Positive hits are indicated by white numerals as follows: 1, Fhl1; 2, EphA4; 3, Rnf130. Data are representative of duplicate RNAi screens for 140 genes performed in triplicate.

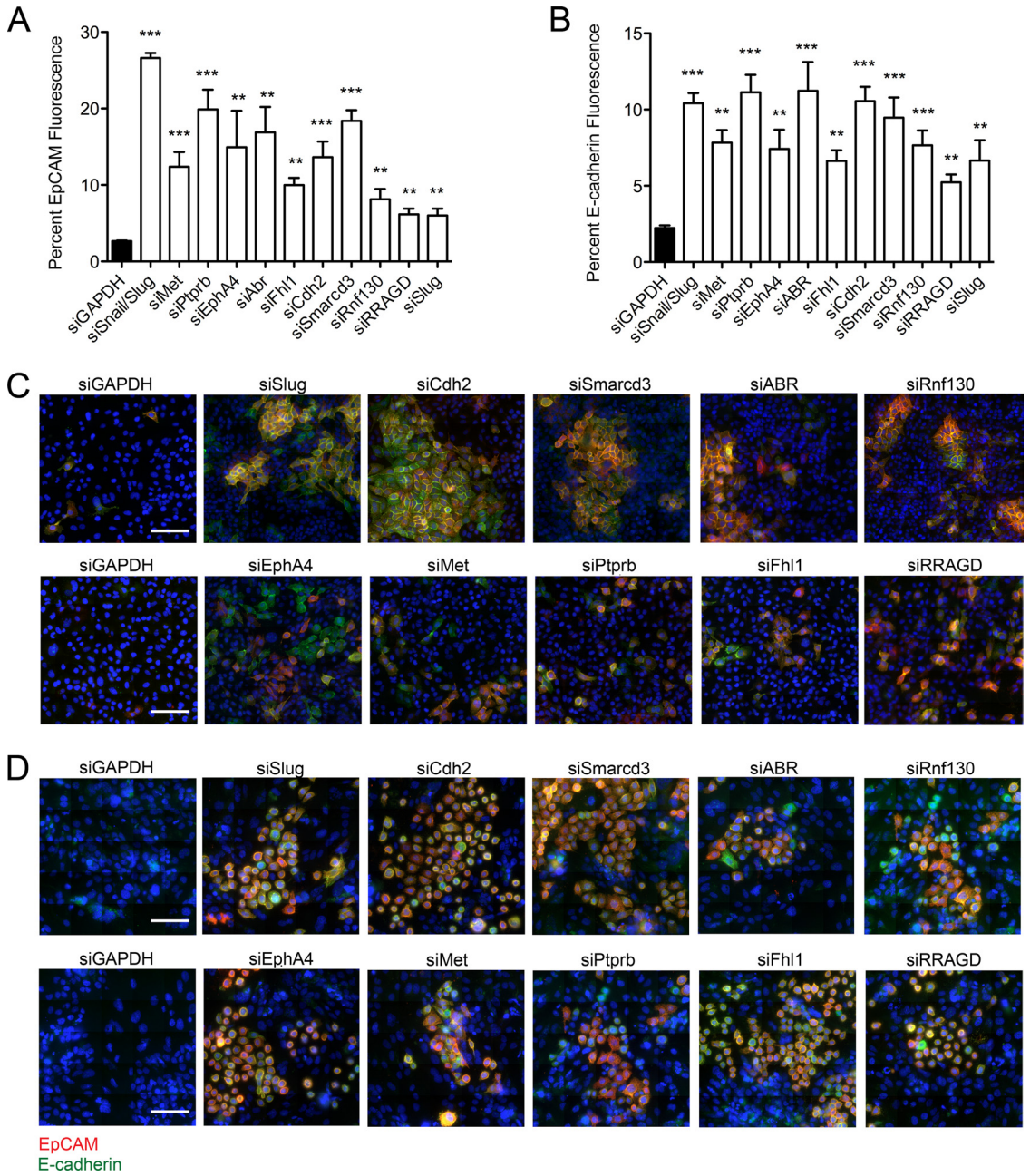

FIG 3 RNAi screen identifies genes important for EMT. (A and B) Elevated EpCAM and E-cadherin percent cellular fluorescence quantitated on a single-cell basis following siRNA-mediated knockdown of the genes indicated. Values are means plus SEMs of 6 independent wells from the primary screen. Statistical significance was evaluated by an unpaired Student's *t* test and indicated as follows: ***, *P* value < 0.001; **, *P* value < 0.01. (C and D) Acquisition of the epithelial phenotype by mesenchymal EpCAM$^-$ cells following siRNA-mediated knockdown of the genes indicated is shown by immunostaining of SUM149 (C) and SUM229 (D) EpCAM$^-$ cells with nuclear DAPI (blue) stain, anti-E-cadherin (green), and anti-EpCAM (red) antibodies. Bars, 100 μm.

or EpCAM expression (Fig. 7A). Immunofluorescence, Western blotting, and qRT-PCR analysis of D3- and Slug-HMECs showed decreased E-cadherin and increased vimentin, N-cadherin, and fibronectin expression (Fig. 7A to C), while Snail-HMECs had preferentially decreased EpCAM expression (Fig. 7A and B). Both Snail- and Slug-HMECs had a 2- to 4-fold increase in Smarcd3/Baf60c mRNA expression (Fig. 7C). Snail- and Slug-HMECs also had increased mRNA levels for the EMT-inducing transcription factor Zeb2 similar to Smarcd3/Baf60c (Fig. 5F and 7D). Like D3-HMECs, Slug-HMECs preferentially repressed the cell-cell adhesion tight junction genes Cldn4 and Cldn7, possibly contributing to the disruption of epithelial cell polarity (Fig. 7E). Cumulatively, these findings suggest that Smarcd3/Baf60c and Slug impact an overlapping EMT network.

SWI/SNF complex regulates WNT signaling through induction of Wnt5a expression. Wnt5a regulates cellular polarity and cell-cell adhesion through activation of noncanonical WNT signaling pathways (25–27). Expression of Wnt5a was upregulated in

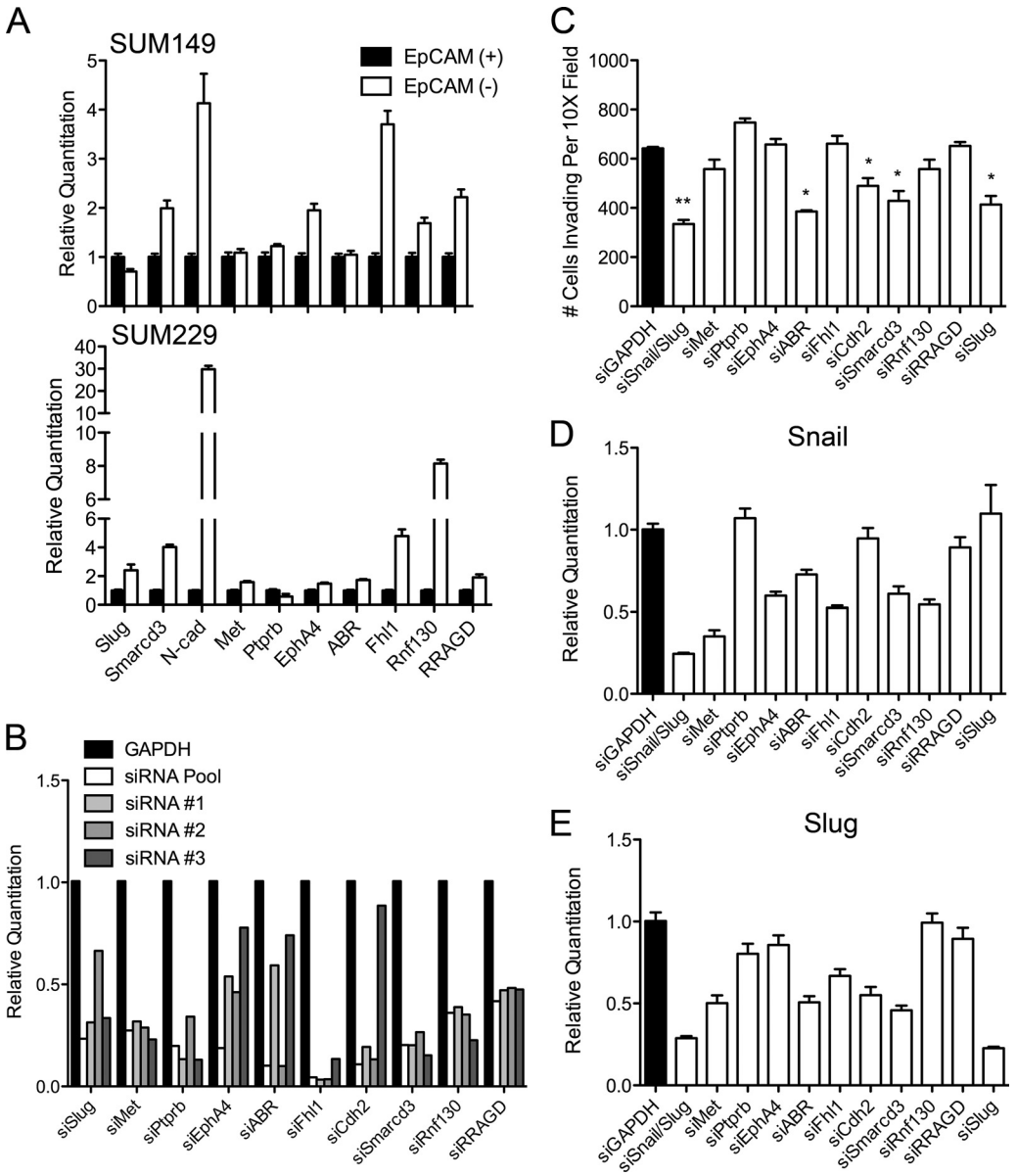

FIG 4 EMT regulatory genes affect cellular invasiveness and expression of EMT-inducing transcription factors. (A) Expression levels of EMT regulatory genes in EpCAM$^{+/high}$ cells compared to EpCAM^{-} cells measured by qRT-PCR. N-cad, N-cadherin. (B) Deconvolution of siRNA smart pools demonstrates knockdown of EMT regulatory genes with at least two individual siRNA oligonucleotides per gene in SUM149 EpCAM^{-} cells as shown by qRT-PCR. (C) Cellular invasiveness through Matrigel-coated Transwell chambers of SUM149 EpCAM^{-} cells following siRNA-mediated knockdown of the indicated EMT regulatory genes. Statistical significance was evaluated by an unpaired Student's *t* test and indicated as follows: **, *P* value < 0.01; *, *P* value < 0.05. Values are means plus SEMs of two independent experiments performed in triplicate. (D and E) Expression changes of EMT-inducing transcription factors in EpCAM^{-} SUM149 cells following siRNA-mediated knockdown of the indicated EMT regulatory genes measured by qRT-PCR. The values in panels A, B, D, and E are means plus SEMs of at least three independent experiments performed in triplicate.

two independent D3-HMEC lines (Fig. 8A; see Table S4 in supplemental material). Activation of Wnt5a-regulated signaling pathways in D3-HMECs was demonstrated by increased PKCβ phosphorylation and expression of TGFβ (Fig. 8A and B). Nuclear localization of β-catenin was decreased in the D3-HMECs, suggesting decreased β-catenin function associated with Smarcd3/Baf60c expression (Fig. 8B).

The ATP-dependent catalytic components of multisubunit SWI/SNF chromatin-remodeling complexes are either Brm or Brg1 (20). In D3-HMECs, Brg1 expression was increased and co-immunoprecipitated with FLAG-Smarcd3/Baf60c (Fig. 8C and D). Chromatin immunoprecipitation (ChIP) assays were used to determine whether the Brg1/Smarcd3/Baf60c complex resided on the Wnt5a gene promoter (Fig. 8E). Brg1 regulates transcription of E-cadherin and Cd44 (28), so we used these genes as controls for ChIP assays. Smarcd3/Baf60c and Brg1 bound to the promoters of E-cadherin, Cd44, and Wnt5a genes but not to the promoter of the Cldn4 gene (Fig. 8E and F). Parallel ChIP assays for the histone methylation mark H3K4me3, which correlates with active transcription, showed loss of this histone mark on the promoters

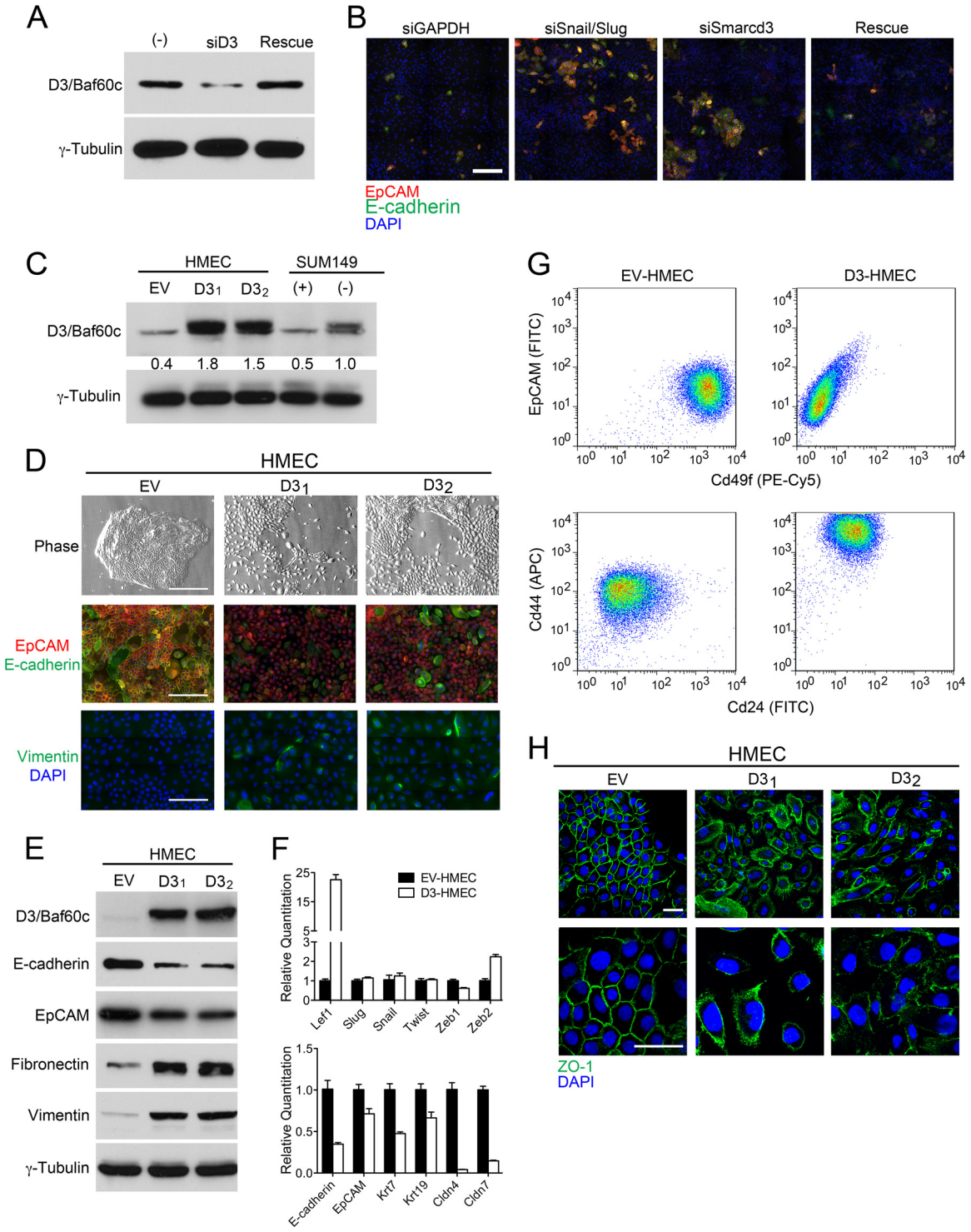

FIG 5 Smarcd3/Baf60c is an epigenetic regulator of EMT. (A) Western blot comparing levels of expression of Smarcd3/Baf60c in EpCAM$^-$ SUM149 cells before (−) and after siRNA-mediated knockdown of Smarcd3 (siD3) and following the rescue of Smarcd3 expression. (B) Mesenchymal EpCAM$^-$ cells do not acquire the epithelial phenotype following the rescue of Smarcd3 expression as shown by immunostaining with nuclear DAPI (blue) stain, anti-E-cadherin (green) and anti-EpCAM (red) antibodies. Representative images of two independent experiments performed in quadruplicate are shown. Bar, 100 μm. (C) Expression of Smarcd3/Baf60c in HMECs at levels comparable to those in EpCAM$^-$ SUM149 cells. EV, empty vector; $D3_1$ and $D3_2$, two independent HMEC clones expressing Baf60c. (D) Smarcd3/Baf60c-expressing HMECs (D3-HMECs) gain a mesenchymal phenotype with loss of epithelial properties as shown by phase microscopy and immunostaining of EV- and D3-HMECs with nuclear DAPI (blue) stain, anti-E-cadherin (green), anti-EpCAM (red), or antivimentin (green) antibodies. Bars, 500 μm. (E) Loss of epithelial markers EpCAM and E-cadherin and gain of mesenchymal markers fibronectin and vimentin in D3-HMECs shown by Western blotting. (F) Elevated mRNA expression of EMT-inducing transcription factors Lef1 and Zeb2 and reduced expression of epithelial and cell adhesion markers in D3-HMECs measured by qRT-PCR. Values are means plus SEMs of three independent experiments performed in triplicate. (G) Different antigenic profiles in EV- versus D3-HMECs demonstrated by FACS analysis with epithelial differentiation markers anti-EpCAM (FITC) and anti-Cd49f (PE-Cy5) or cancer stem-like markers anti-Cd44 (APC) and anti-Cd24 (FITC). (H) Loss of epithelial cell polarity in D3-HMECs shown by confocal microscopy of EV- and D3-HMECs stained with nuclear DAPI (blue) stain and anti-ZO1 (green) antibody. Images are representative of at least two independent experiments. Bars, 50 μm.

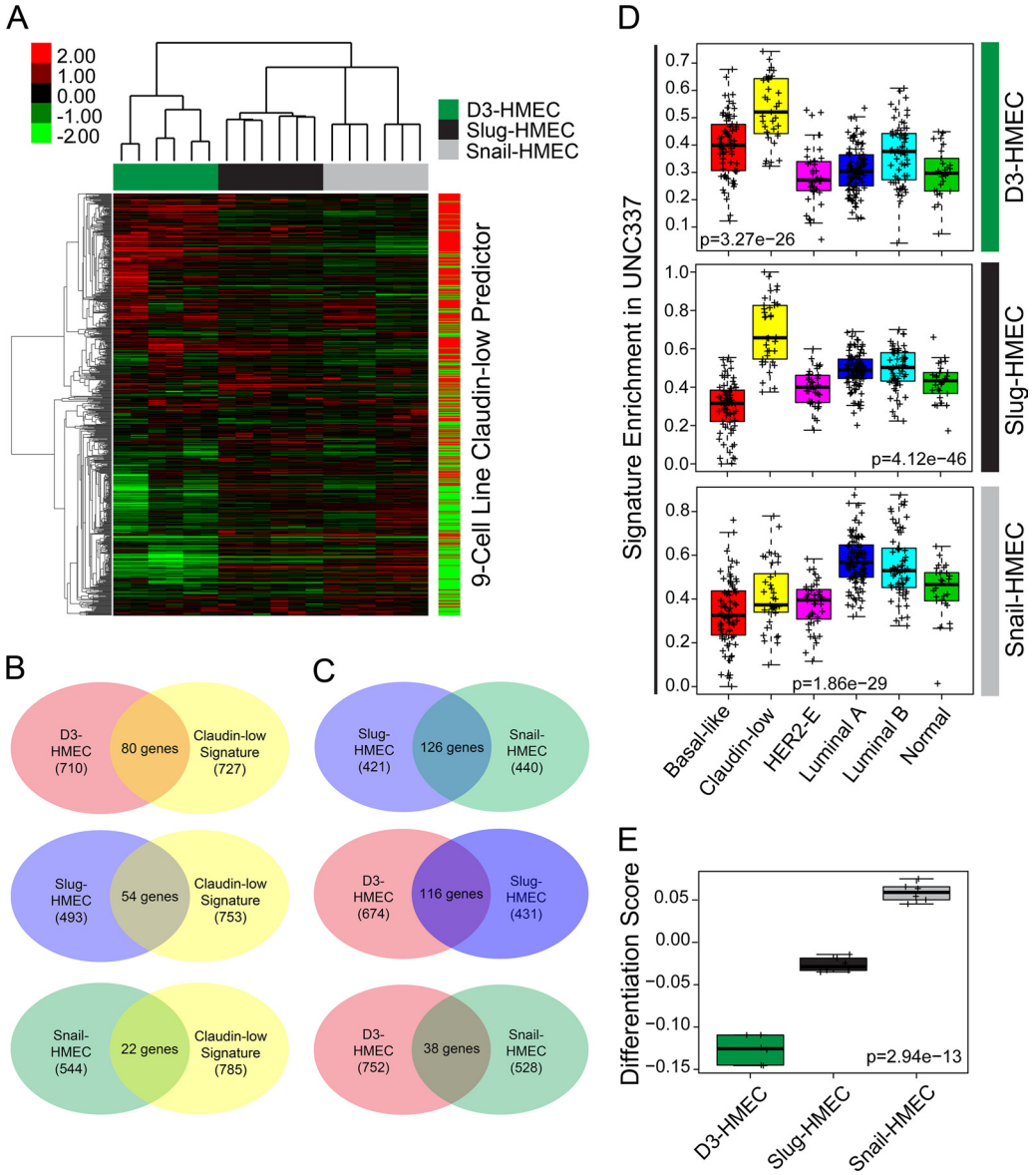

FIG 6 Smarcd3/Baf60c expression induces a claudin-low gene signature. (A) Gene expression profiles of D3-HMECs cluster with the claudin-low gene signature. Heat map compares gene expression of D3-HMECs, Slug-HMECs, and Snail-HMECs to the 9-cell line claudin-low predictor. Upregulated genes (red) and downregulated genes (green) are indicated. (B and C) Venn diagrams depict shared genes between D3-, Slug-, and Snail-HMECs compared to the claudin-low predictor or compared to each other. (D) Claudin-low human tumors show the highest expression of D3-HMEC genes among breast cancer subtypes, as demonstrated by the mean expression of D3-, Slug-, and Snail-HMEC genes across the subtypes of breast cancer in the UNC337 data set. *P* values were calculated by comparing gene expression means across all subtypes using an analysis of variance (ANOVA) test. Each plus symbol represents a distinct tumor sample within the data set. (E) Differentiation scores compare D3-, Slug-, and Snail-HMECs relative to EV-HMECs showing the lowest differentiation propensity of D3-HMECs. The *P* value was calculated by comparing gene expression means across all breast epithelial cell lineages.

of repressed E-cadherin and Cldn4 genes and gain on the promoters of induced Cd44 and Wnt5a genes (Fig. 7G). Cumulatively, the findings indicate that Smarcd3/Baf60c and Brg1 bind the Wnt5a promoter for the activation of Wnt5a transcription.

Inhibition of Wnt5a restores the epithelial phenotype. Similar elevation of Wnt5a expression was observed in Slug-HMECs and EpCAM$^-$ SUM149 and SUM229 cells, supporting a role for Wnt5a in the induction of EMT in these cells with upregulated Smarcd3/Baf60c expression (Fig. 9A and B). To determine whether Wnt5a was responsible for inducing the loss of epithelial characteristics resulting from Smarcd3/Baf60c expression, we inhibited Wnt5a expression using RNAi in D3-HMECs. siRNA-mediated knockdown of Wnt5a phenotypically converted mesenchymal-like cells lacking cell-cell adhesions to epithelial colonies with a cobblestone morphology (Fig. 9C). Wnt5a knockdown resulted in the increased mRNA and protein expression of epithelial markers E-cadherin and EpCAM (Fig. 9D and E). Although expression of epithelial tight junction genes Cldn4 and Cldn7 was reduced by 90% in D3-HMECs relative to EV-HMECs (Fig. 5F), knockdown of Wnt5a in D3-HMECs resulted in a 10-fold increase in Cldn4 and Cldn7 (Fig. 9D). The EMT-inducing transcription factor Lef1 and the mesenchymal marker vimentin, which were each induced

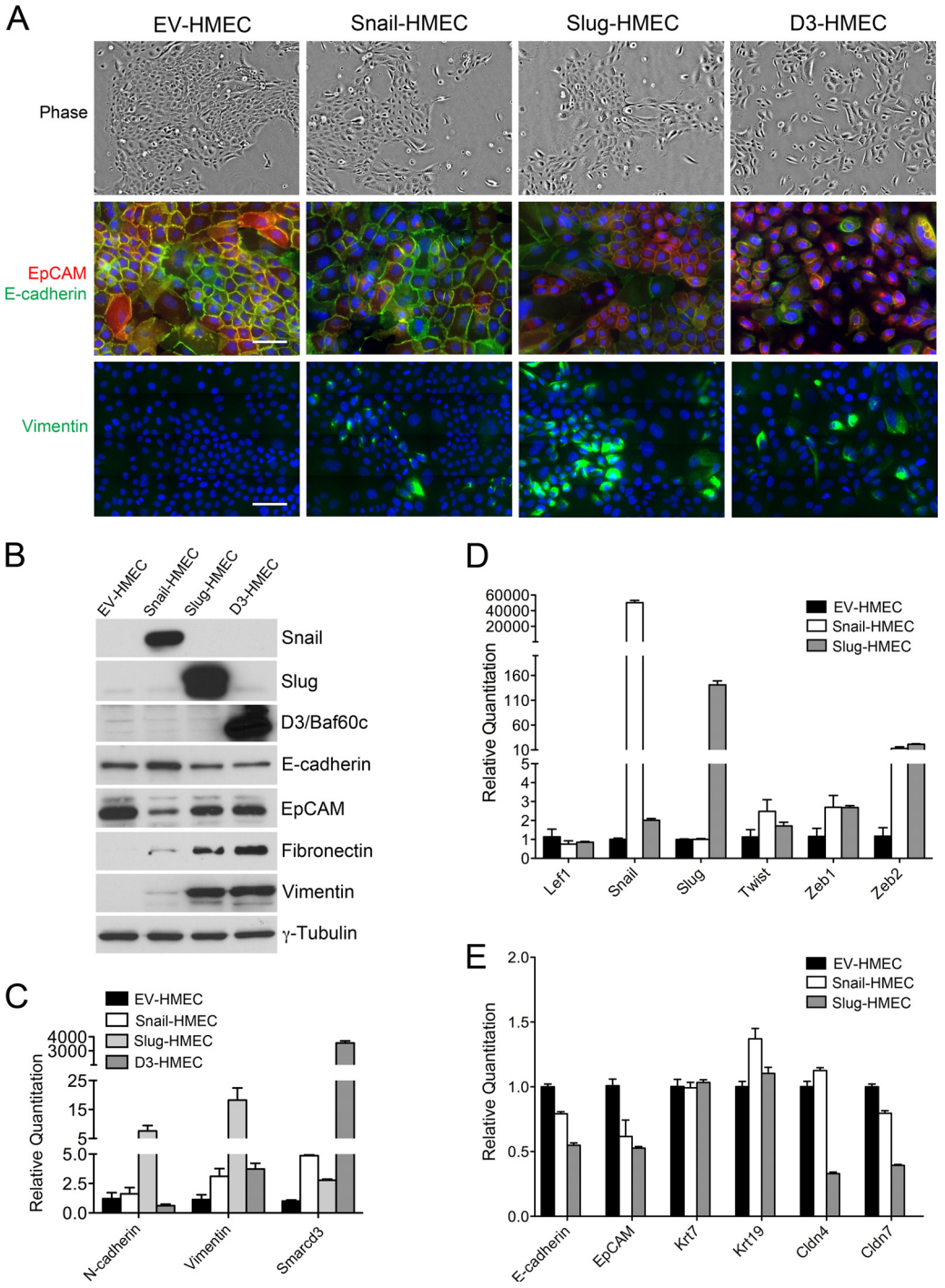

FIG 7 Phenotypic comparison of Snail-, Slug-, and Smarcd3-induced EMT. (A) Loss of the epithelial phenotype with gain of mesenchymal properties in D3-, Slug-, and/or Snail-HMECs as shown by phase microscopy and immunostaining with nuclear DAPI (blue) stain, anti-E-cadherin (green), and anti-EpCAM (red) antibodies. (B) Western blotting shows reduced protein expression for epithelial markers EpCAM or E-cadherin and elevated protein expression of mesenchymal markers fibronectin and vimentin in Snail-, Slug-, and D3-HMECs. (C) Elevated gene expression of mesenchymal markers N-cadherin, vimentin, and Smarcd3/Baf60c in Snail-, Slug-, and D3-HMECs measured by qRT-PCR. (D and E) Elevated gene expression of EMT-inducing transcription factors and reduced expression of epithelial cell-cell adhesion markers in Snail- and Slug-HMECs measured by qRT-PCR. Values are means plus SEMs of three independent experiments performed in triplicate. The images in panel A and data in panels B and C are representative of the results of at least two independent experiments.

with Smarcd3/Baf60c expression (Fig. 5D and E), were repressed with knockdown of Wnt5a (Fig. 9D). Knockdown of Wnt5a repressed PKCβ phosphorylation, consistent with inhibition of the WNT signaling pathway (Fig. 9E). Treatment of D3-HMECs with a Wnt5a blocking antibody inhibited cellular invasiveness by 70% compared to untreated D3-HMECs (Fig. 9F), demonstrating that the phenotypic changes coincided with functional changes indicative of a more epithelial cell state. Functionally, the blocking an-

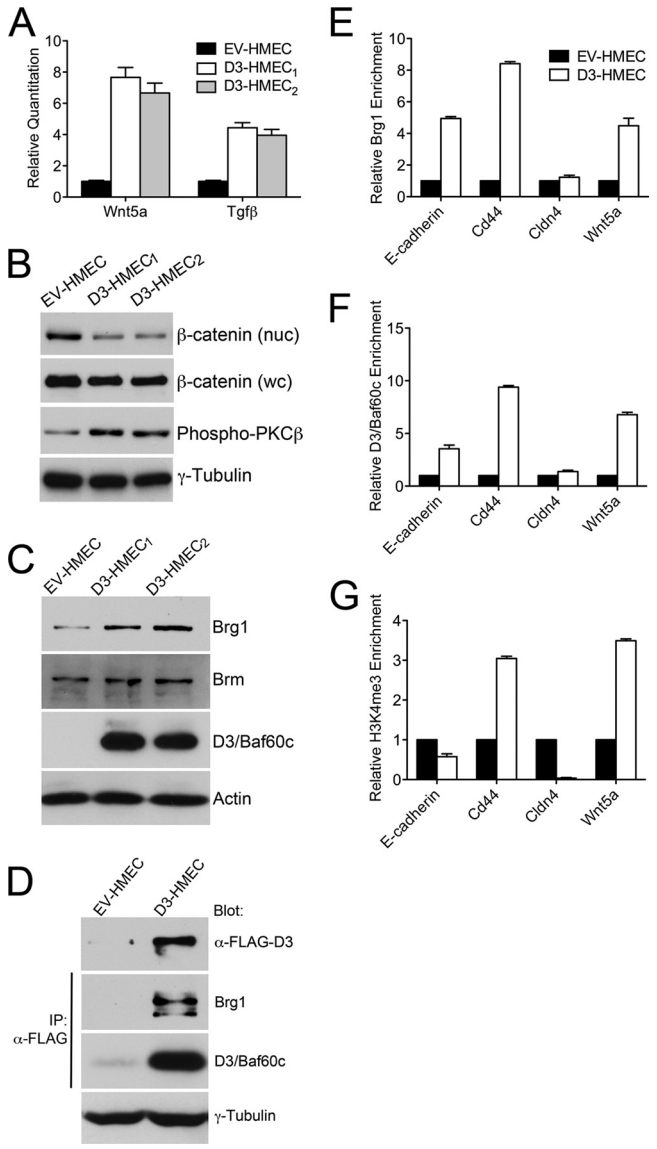

FIG 8 SWI/SNF complex regulates noncanonical WNT signaling through induction of Wnt5a expression. (A) Elevated expression of Wnt5a and TGFβ in D3-HMECs shown by qRT-PCR. Values are means plus SEMs of three independent experiments performed in triplicate. (B) Activation of noncanonical WNT signaling with inhibition of canonical WNT signaling shown by Western blotting for elevated phosphorylation of PKCβ and reduced nuclear (nuc) but not whole-cell (wc) β-catenin protein expression. (C) Induced Brg1 protein expression with the expression of Smarcd3/Baf60c in HMECs shown by Western blotting with the antibodies indicated. (D) Brg1 coimmunoprecipitates with FLAG-Smarcd3/Baf60c in HMECs. IP, immunoprecipitation; α-FLAG, anti-FLAG antibody. The results shown in panels B to D are representative of at least two independent experiments. (E to G) Elevated Smarcd3/Baf60c, Brg1, and H3K4me3 on the promoters of the indicated genes in D3-HMECs compared to EV-HMECs as measured by ChIP–qRT-PCR. Values are means plus SEMs of three independent experiments performed in duplicate.

tibody was as effective as siRNA-mediated knockdown of Wnt5a. These results demonstrated that Smarcd3/Baf60c promoted EMT in D3-HMECs by promoting Wnt5a expression.

DISCUSSION

We describe a directed phenotypic RNAi screen that identified genes whose individual knockdown was sufficient to promote MET in the EpCAM$^-$ population of SUM149 and SUM229 breast cancer cells. While it has long been accepted that EMT is a reversible process during development, few studies have examined the opposite process of MET (3, 5). Our RNAi screen targeted 140 genes from an EMT gene signature shared by epithelial stem cells developmentally entering EMT and claudin-low breast cancer cells with properties of EMT and stemness (9). Ten of the 140 genes were identified as EMT regulatory genes, whose individual siRNA-mediated knockdown was sufficient to promote MET. Three of the genes, Slug, Met receptor tyrosine kinase, and N-cadherin, are well-defined regulators of EMT and provide validation of the screen (1). The other seven genes have no defined role in EMT. The functions of the seven genes do suggest their potential importance in the phenotypic reprogramming associated with EMT. For instance, EphA4 and Ptprb/VE-Ptp represent a receptor tyrosine kinase and phosphatase, respectively, that in development have been shown to be critical regulators of angiogenesis (29–32). Fhl1 localizes to focal adhesions where it promotes cell spreading in a TGFβ-dependent manner, and Rnf130 is a ring finger protein with putative E3 ligase activity (33–37). Consistent with its knockdown inhibiting invasion of mesenchymal EpCAM$^-$ SUM149 cells, ABR is a guanine nucleotide exchange factor (GEF)/GTPase-activating protein (GAP) for Rho and Cdc42 GTPases, and RRAGD is a poorly characterized GTPase with homology to Ras (38–41). Among these genes, Rnf130 is an interesting gene candidate for future studies with respect to EMT. Our preliminary findings have demonstrated that combined knockdown of Rnf130, Slug, and Smarcd3/Baf60c produced synergistic effects in promoting an epithelial morphology in fully mesenchymal claudin-low SUM159 breast cancer cells. As a putative E3 ligase, there are no defined substrates for ubiquitination by Rnf130. The findings are suggestive that these genes, in addition to Slug, Met, N-cadherin, and Smarcd3/Baf60c, are likely members of a signaling network controlling EMT.

We demonstrated that Smarcd3/Baf60c is a novel epigenetic EMT regulatory gene. Smarcd3/Baf60c was the only gene identified in the RNAi screen whose knockdown strongly increased both EpCAM and E-cadherin expression, decreased Snail and Slug expression, inhibited invasiveness, and was also upregulated in EpCAM$^-$ cells relative to EpCAM$^{+/high}$ SUM149 and SUM229 breast cancer cells. Smarcd3/Baf60c as a member of the multisubunit ATP-dependent SWI/SNF chromatin-remodeling complex has the ability to epigenetically modulate gene expression programs (20, 21). Smarcd3/Baf60c induced an EMT gene expression program in HMECs, indicating that Smarcd3/Baf60c plays an important role in promoting the EMT properties and mesenchymal phenotype of these cells. Consistent with their related roles as transcriptional regulators, siRNA-mediated knockdown of Slug induced a MET similar to inhibition of Smarcd3/Baf60c expression. Notably, ectopic expression of either Smarcd3/Baf60c or Slug similarly induced the expression of Wnt5a, suggesting that Smarcd3/Baf60c affects an EMT gene network that overlaps with the EMT-inducing function of Slug. To our knowledge, this is the first report of Smarcd3/Baf60c promoting an epigenetic reprogramming event responsible for inducing an EMT in HMECs. Also, Smarcd3/Baf60c maintains the mesenchymal phenotype in claudin-low EpCAM$^-$ populations of SUM149 and SUM229 cells.

There is an expanding awareness that SWI/SNF chromatin-remodeling complexes play critical functions in reprogramming events relevant to EMT and lineage commitment. Brg1, one of the

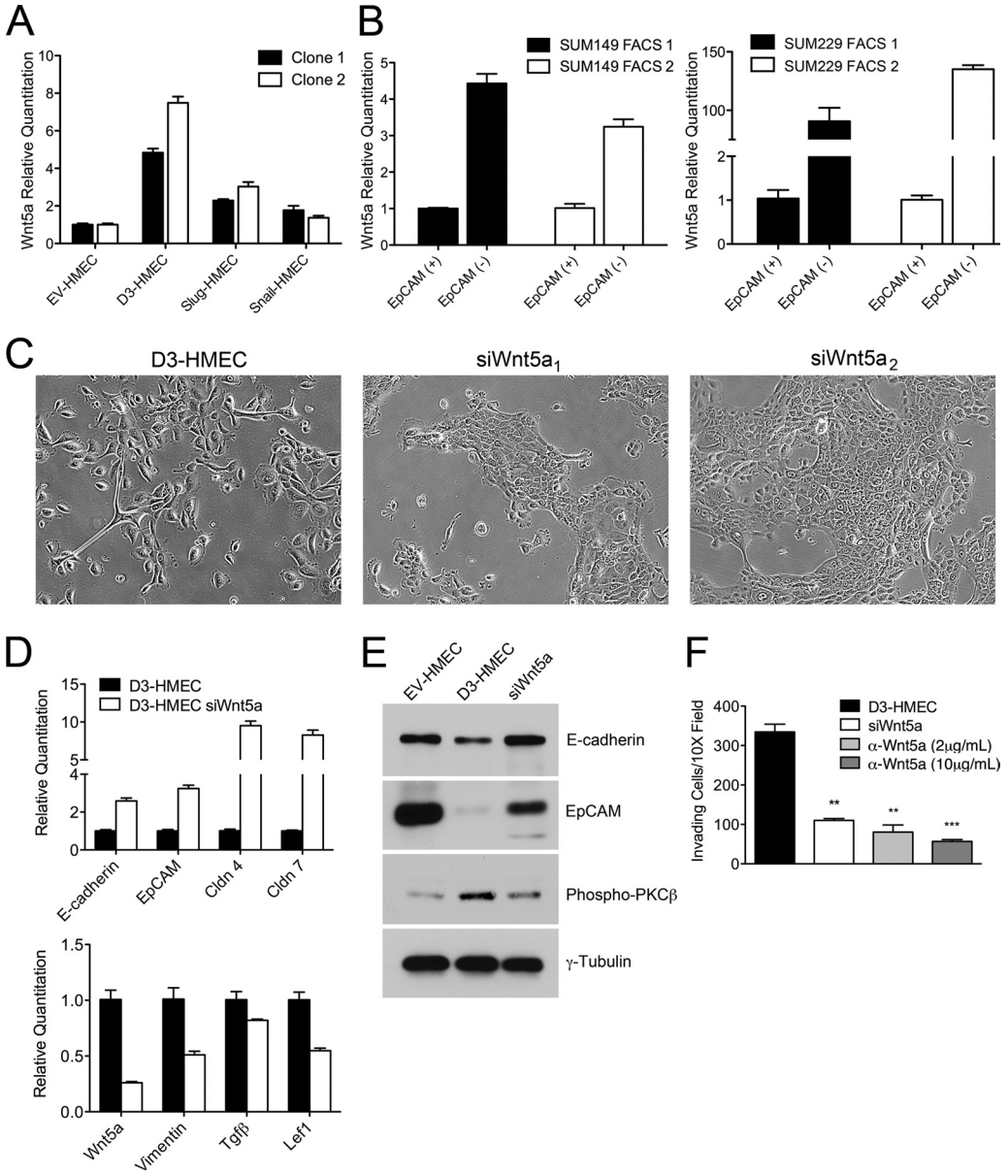

FIG 9 Inhibition of Wnt5a restores epithelial adherens junctions. (A) Wnt5a expression correlates with the mesenchymal phenotype of EpCAM$^-$ cells. Elevated gene expression of Wnt5a in Slug-HMECs is similar to D3-HMECs measured by qRT-PCR. (B) Elevated gene expression of Wnt5a in EpCAM$^-$ SUM149 and SUM229 cells compared to EpCAM$^{+/high}$ SUM149 and SUM229 cells measured by qRT-PCR from two independent FACS sorts. Values in panels A and B are means plus SEMs of two independent experiments performed in triplicate. (C) siRNA-mediated knockdown of Wnt5a partially restores the epithelial phenotype of D3-HMECs as shown by phase microscopy. (D) siRNA-mediated knockdown of Wnt5a increases mRNA expression of epithelial and cell-cell adhesion markers and decreases expression of the mesenchymal marker vimentin and the EMT-inducing transcription factor Lef1. Data are measured by qRT-PCR, and values are means plus SEMs of three independent experiments performed in triplicate. (E) Western blotting showing increased protein expression of EpCAM and E-cadherin with loss of PKCβ phosphorylation in D3-HMECs transfected with siWnt5a. (F) Reduced invasiveness through growth factor-reduced Matrigel-coated Transwell chambers of D3-HMECs treated with siWnt5a or two different concentrations of the Wnt5a blocking antibody (α-Wnt5a) compared to untreated D3-HMECs. Statistical significance was evaluated by an unpaired Student's *t* test and indicated as follows: ***, *P* value < 0.001; **, *P* value < 0.01. Values are means plus SEMs of two independent experiments performed in triplicate.

catalytic components of SWI/SNF chromatin-remodeling complex, is important in the reprogramming of somatic cells to induced pluripotent stem (iPS) cells (42, 43). MET was shown recently to occur simultaneously with the reprogramming of fibroblasts to iPS cells, directly connecting MET to iPS cell generation (44). Our results indicate that studies are warranted to determine whether Smarcd3/Baf60c expression is repressed in these cells as a switch to induce MET during iPS cell reprogramming. In the context of regulating EMT and MET, WNT signaling has been shown to be an important collaborator with TGFβ for inducing EMT. WNT signaling, for example, contributes to the metastatic progression of pancreatic cancer and melanoma (45–47). In D3-HMECs, we showed that both Smarcd3/Baf60c and Brg1 bind the promoters of Wnt5a and E-cadherin. Wnt5a expression is in-

duced, stimulating WNT signaling, while E-cadherin expression is repressed to promote EMT. Together, these findings show the importance of Smarcd3/Baf60c in controlling the commitment to the mesenchymal cellular phenotype. Further studies are warranted to determine the function of SWI/SNF-regulated epigenetic changes that contribute to the claudin-low subtype of breast cancer.

ACKNOWLEDGMENTS

G.L.J. is supported by NIH grant GM101141 and the University Cancer Research Fund. N.V.J. was supported by NIH training grant GM007040. We thank the UNC Flow Cytometry and RNAi Core Facilities, which are supported in part by an NCI Center Core Support Grant (P30CA06086) to the UNC Lineberger Comprehensive Cancer Center.

We thank Ben Major (UNC—Chapel Hill) and Lorenzo Puri (Sanford Burnham Medical Research Institute) for the lentiviral FLAG-Gateway destination vector and the Smarcd3/Baf60c antibody, respectively.

We declare that we have no conflicts of interest.

REFERENCES

1. **Thiery JP, Sleeman JP.** 2006. Complex networks orchestrate epithelial–mesenchymal transitions. Nat. Rev. Mol. Cell Biol. **7:**131–142.
2. **Yang J, Weinberg RA.** 2008. Epithelial-mesenchymal transition: at the crossroads of development and tumor metastasis. Dev. Cell **14:**818–829.
3. **Valastyan S, Weinberg RA.** 2011. Tumor metastasis: molecular insights and evolving paradigms. Cell **147:**275–292.
4. **Thiery JP, Acloque H, Huang RYJ, Nieto MA.** 2009. Epithelial-mesenchymal transitions in development and disease. Cell **139:**871–890.
5. **Kalluri R, Weinberg RA.** 2009. The basics of epithelial-mesenchymal transition. J. Clin. Invest. **119:**1420–1428.
6. **Nieto MA.** 2011. The ins and outs of the epithelial to mesenchymal transition in health and disease. Annu. Rev. Cell Dev. Biol. **27:**347–376.
7. **Kouzarides T.** 2007. Chromatin modifications and their function. Cell **128:**693–705.
8. **Nieto MA.** 2002. The Snail superfamily of zinc-finger transcription factors. Nat. Rev. Mol. Cell Biol. **3:**155–166.
9. **Abell AN, Jordan NV, Huang W, Prat A, Midland AA, Johnson NL, Granger DA, Mieczkowski PA, Perou CM, Gomez SM, Li L, Johnson GL.** 2011. MAP3K4/CBP-regulated H2B acetylation controls epithelial-mesenchymal transition in trophoblast stem cells. Cell Stem Cell **8:**525–537.
10. **Fulford LG, Reis-Filho JS, Ryder K, Jones C, Gillett CE, Hanby A, Easton DF, Lakhani SR.** 2007. Basal-like grade III invasive ductal carcinoma of the breast: patterns of metastasis and long term survival. Breast Cancer Res. **9:**R4. doi:10.1186/bcr1636.
11. **Gaedcke J, Traub F, Milde S, Wilkens L, Stan A, Ostertag H, Christgen M, von Wasielewski R, Kreipe HH.** 2007. Predominance of the basal type and HER-2/neu type in brain metastasis from breast cancer. Mod. Pathol. **20:**864–870.
12. **Banerjee S.** 2006. Basal-like breast carcinomas: clinical outcome and response to chemotherapy. J. Clin. Pathol. **59:**729–735.
13. **Prat A, Parker JS, Karginova O, Fan C, Livasy C, Herschkowitz JI, He X, Perou CM.** 2010. Phenotypic and molecular characterization of the claudin-low intrinsic subtype of breast cancer. Breast Cancer Res. **12:**R68. doi:10.1186/bcr2635.
14. **Gupta PB, Fillmore CM, Jiang G, Shapira SD, Tao K, Kuperwasser C, Lander ES.** 2011. Stochastic state transitions give rise to phenotypic equilibrium in populations of cancer cells. Cell **146:**633–644.
15. **Proia TA, Keller PJ, Gupta PB, Klebba I, Jones AD, Sedic M, Gilmore H, Tung N, Naber SP, Schnitt S, Lander ES, Kuperwasser C.** 2011. Genetic predisposition directs breast cancer phenotype by dictating progenitor cell fate. Cell Stem Cell **8:**149–163.
16. **Troester MA.** 2004. Cell-type-specific responses to chemotherapeutics in breast cancer. Cancer Res. **64:**4218–4226.
17. **Abell AN, Granger DA, Johnson NL, Vincent-Jordan N, Dibble CF, Johnson GL.** 2009. Trophoblast stem cell maintenance by fibroblast growth factor 4 requires MEKK4 activation of Jun N-terminal kinase. Mol. Cell. Biol. **29:**2748–2761.
18. **Hu Z, Fan C, Oh DS, Marron JS, He X, Qaqish BF, Livasy C, Carey LA, Reynolds E, Dressler L, Nobel A, Parker J, Ewend MG, Sawyer LR, Wu J, Liu Y, Nanda R, Tretiakova M, Orrico A, Dreher D, Palazzo JP, Perreard L, Nelson E, Mone M, Hansen H, Mullins M, Quackenbush JF, Ellis MJ, Olopade OI, Bernard PS, Perou CM.** 2006. The molecular portraits of breast tumors are conserved across microarray platforms. BMC Genomics **7:**96–108. doi:10.1186/1471-2164-7-96.
19. **Eisen MB, Spellman PT, Brown PO, Botstein D.** 1998. Cluster analysis and display of genome-wide expression patterns. Proc. Natl. Acad. Sci. U. S. A. **95:**14863–14868.
20. **Ho L, Crabtree GR.** 2010. Chromatin remodelling during development. Nature **463:**474–484.
21. **Lickert H, Takeuchi JK, Von Both I, Walls JR, McAuliffe F, Adamson SL, Henkelman RM, Wrana JL, Rossant J, Bruneau BG.** 2004. Baf60c is essential for function of BAF chromatin remodelling complexes in heart development. Nature **432:**107–112.
22. **Takeuchi JK, Lickert H, Bisgrove BW, Sun X, Yamamoto M, Chawengsaksophak K, Hamada H, Yost HJ, Rossant J, Bruneau BG.** 2007. Baf60c is a nuclear Notch signaling component required for the establishment of left-right asymmetry. Proc. Natl. Acad. Sci. U. S. A. **104:**846–851.
23. **Forcales SV, Albini S, Giordani L, Malecova B, Cignolo L, Chernov A, Coutinho P, Saccone V, Consalvi S, Williams R, Wang K, Wu Z, Baranovskaya S, Miller A, Dilworth FJ, Puri PL.** 2011. Signal-dependent incorporation of MyoD-BAF60c into Brg1-based SWI/SNF chromatin-remodelling complex. EMBO J. **2:**301–316.
24. **Lim E, Vaillant F, Wu D, Forrest NC, Pal B, Hart AH, Asselin-Labat M-L, Gyorki DE, Ward T, Partanen A, Feleppa F, Huschtscha LI, Thorne HJ, kConFab, Fox SB, Yan M, French JD, Brown MA, Smyth GK, Visvader JE, Lindeman GJ.** 2009. Aberrant luminal progenitors as the candidate target population for basal tumor development in BRCA1 mutation carriers. Nat. Med. **15:**907–915.
25. **Veeman MT, Axelrod JD, Moon RT.** 2003. A second canon. Functions and mechanisms of beta-catenin-independent Wnt signaling. Dev. Cell **5:**367–377.
26. **Zhu Y, Tian Y, Du J, Hu Z, Yang L, Liu J, Gu L.** 2012. Dvl2-dependent activation of Daam1 and RhoA regulates Wnt5a-induced breast cancer cell migration. PLoS One **7:**e37823. doi:10.1371/journal.pone.0037823.
27. **Dissanayake SKS, Wade MM, Johnson CEC, O'Connell MPM, Leotlela PDP, French ADA, Shah KVK, Hewitt KJK, Rosenthal DTD, Indig FEF, Jiang YY, Nickoloff BJB, Taub DDD, Trent JMJ, Moon RTR, Bittner MM, Weeraratna ATA.** 2007. The Wnt5A/protein kinase C pathway mediates motility in melanoma cells via the inhibition of metastasis suppressors and initiation of an epithelial to mesenchymal transition. J. Biol. Chem. **282:**17259–17271.
28. **Banine F.** 2005. SWI/SNF chromatin-remodeling factors induce changes in DNA methylation to promote transcriptional activation. Cancer Res. **65:**3542–3547.
29. **Holder N, Klein R.** 1999. Eph receptors and ephrins: effectors of morphogenesis. Development **126:**2033–2044.
30. **Pasquale EB.** 2010. Eph receptors and ephrins in cancer: bidirectional signalling and beyond. Nat. Rev. Cancer **10:**165–180.
31. **Dominguez MG, Hughes VC, Pan L, Simmons M, Daly C, Anderson K, Noguera-Troise I, Murphy AJ, Valenzuela DM, Davis S, Thurston G, Yancopoulos GD, Gale NW.** 2007. Vascular endothelial tyrosine phosphatase (VE-PTP)-null mice undergo vasculogenesis but die embryonically because of defects in angiogenesis. Proc. Natl. Acad. Sci. U. S. A. **104:**3243–3248.
32. **Mori M, Murata Y, Kotani T, Kusakari S, Ohnishi H, Saito Y, Okazawa H, Ishizuka T, Mori M, Matozaki T.** 2010. Promotion of cell spreading and migration by vascular endothelial-protein tyrosine phosphatase (VE-PTP) in cooperation with integrins. J. Cell. Physiol. **224:**195–204.
33. **Rafael MS, Laizé V, Florindo C, Ferraresso S, Bargelloni L, Cancela ML.** 2012. Overexpression of four and a half LIM domains protein 2 promotes epithelial-mesenchymal transition-like phenotype in fish pre-osteoblasts. Biochimie **94:**1128–1134.
34. **Maetzel D, Denzel S, Mack B, Canis M, Went P, Benk M, Kieu C, Papior P, Baeuerle PA, Munz M, Gires O.** 2009. Nuclear signalling by tumour-associated antigen EpCAM. Nat. Cell Biol. **11:**162–171.
35. **Ding L, Wang Z, Yan J, Yang X, Liu A, Qiu W, Zhu J, Han J, Zhang H, Lin J, Cheng L, Qin X, Niu C, Yuan B, Wang X, Zhu C, Zhou Y, Li J, Song H, Huang C, Ye Q.** 2009. Human four-and-a-half LIM family members suppress tumor cell growth through a TGF-β–like signaling pathway. J. Clin. Invest. **119:**349–361.
36. **Sheikh F, Raskin A, Chu P-H, Lange S, Domenighetti AA, Zheng M,**

Liang X, Zhang T, Yajima T, Gu Y, Dalton ND, Mahata SK, Dorn GW, II, Heller-Brown J, Peterson KL, Omens JH, McCulloch AD, Chen J. 2008. An FHL1-containing complex within the cardiomyocyte sarcomere mediates hypertrophic biomechanical stress responses in mice. J. Clin. Invest. **118:**3870–3880.

37. **Guais A, Siegrist S, Solhonne B, Jouault H, Guellaën G, Bulle F.** 2006. h-Goliath, paralog of GRAIL, is a new E3 ligase protein, expressed in human leukocytes. Gene **374:**112–120.
38. **Sekiguchi T.** 2001. Novel G proteins, Rag C and Rag D, interact with GTP-binding proteins, Rag A and Rag B. J. Biol. Chem. **276:**7246–7257.
39. **Sancak Y, Bar-Peled L, Zoncu R, Markhard AL, Nada S, Sabatini DM.** 2010. Ragulator-Rag complex targets mTORC1 to the lysosomal surface and is necessary for its activation by amino acids. Cell **141:**290–303.
40. **Tcherkezian J, Lamarche-Vane N.** 2007. Current knowledge of the large RhoGAP family of proteins. Biol. Cell **99:**67–86.
41. **Chuang TH, Xu X, Kaartinen V, Heisterkamp N, Groffen J, Bokoch GM.** 1995. Abr and Bcr are multifunctional regulators of the Rho GTP-binding protein family. Proc. Natl. Acad. Sci. U. S. A. **92:**10282–10286.
42. **Singhal N, Graumann J, Wu G, Araúzo-Bravo MJ, Han DW, Greber B, Gentile L, Mann M, Schöler HR.** 2010. Chromatin-remodeling components of the BAF complex facilitate reprogramming. Cell **141:**943–955.
43. **Kidder BL, Palmer S, Knott JG.** 2009. SWI/SNF-Brg1 regulates self-renewal and occupies core pluripotency-related genes in embryonic stem cells. Stem Cells **27:**317–328.
44. **Li R, Liang J, Ni S, Zhou T, Qing X, Li H, He W, Chen J, Li F, Zhuang Q, Qin B, Xu J, Li W, Yang J, Gan Y, Qin D, Feng S, Song H, Yang D, Zhang B, Zeng L, Lai L, Esteban MA, Pei D.** 2010. A mesenchymal-to-epithelial transition initiates and is required for the nuclear reprogramming of mouse fibroblasts. Cell Stem Cell **7:**51–63.
45. **Scheel C, Eaton EN, Li SH-J, Chaffer CL, Reinhardt F, Kah K-J, Bell G, Guo W, Rubin J, Richardson AL, Weinberg RA.** 2011. Paracrine and autocrine signals induce and maintain mesenchymal and stem cell states in the breast. Cell **145:**926–940.
46. **Yu M, Ting DT, Stott SL, Wittner BS, Ozsolak F, Paul S, Ciciliano JC, Smas ME, Winokur D, Gilman AJ, Ulman MJ, Xega K, Contino G, Alagesan B, Brannigan BW, Milos PM, Ryan DP, Sequist LV, Bardeesy N, Ramaswamy S, Toner M, Maheswaran S, Haber DA.** 2012. RNA sequencing of pancreatic circulating tumour cells implicates WNT signalling in metastasis. Nature **487:**510–513.
47. **Dissanayake SK, Olkhanud PB, O'Connell MP, Carter A, French AD, Camilli TC, Emeche CD, Hewitt KJ, Rosenthal DT, Leotlela PD, Wade MS, Yang SW, Brant L, Nickoloff BJ, Messina JL, Biragyn A, Hoek KS, Taub DD, Longo DL, Sondak VK, Hewitt SM, Weeraratna AT.** 2008. Wnt5A regulates expression of tumor-associated antigens in melanoma via changes in signal transducers and activators of transcription 3 phosphorylation. Cancer Res. **68:**10205–10214.